

Evidential Domain Adaptation for Remaining Useful Life Prediction with Incomplete Degradation

Yubo Hou , Mohamed Ragab , Yucheng Wang , Min Wu , *Senior Member, IEEE*, Abdulla Alseiari ,
Chee-Keong Kwoh , Xiaoli Li, *Fellow, IEEE*, Zhenghua Chen*, *Senior Member, IEEE*

Abstract—Accurate Remaining Useful Life (RUL) prediction without labeled target domain data is a critical challenge, and domain adaptation (DA) has been widely adopted to address it by transferring knowledge from a labeled source domain to an unlabeled target domain. Despite its success, existing DA methods struggle significantly when faced with incomplete degradation trajectories in the target domain, particularly due to the absence of late degradation stages. This missing data introduces a key extrapolation challenge. When applied to such incomplete RUL prediction tasks, current DA methods encounter two primary limitations. First, most DA approaches primarily focus on global alignment, which can misaligns late degradation stage in the source domain with early degradation stage in the target domain. Second, due to varying operating conditions in RUL prediction, degradation patterns may differ even within the same degradation stage, resulting in different learned features. As a result, even if degradation stages are partially aligned, simple feature matching cannot fully align two domains. To overcome these limitations, we propose a novel evidential adaptation approach called EviAdapt, which leverages evidential learning to enhance domain adaptation. The method first segments the source and target domain data into distinct degradation stages based on degradation rate, enabling stage-wise alignment that ensures samples from corresponding stages are accurately matched. To address the second limitation, we introduce an evidential uncertainty alignment technique that estimates uncertainty using evidential learning and aligns the uncertainty across matched stages. The effectiveness of EviAdapt is validated through extensive experiments on the C-MAPSS, N-CMAPSS and PHM2010 datasets. Results show that our approach significantly outperforms state-of-the-art methods, demonstrating its potential for tackling incomplete degradation scenarios in RUL prediction. Our code is available via <https://github.com/keyplay/EviAdapt>.

Index Terms—Domain adaptation, remaining useful life prediction, evidential learning, uncertainty, degradation stage.

I. INTRODUCTION

Prognostics and health management (PHM) of industrial systems and equipment play a crucial role in enhancing reliability, reducing maintenance costs, and improving safety and operational performance [1]. Within the PHM domain, Remaining Useful Life (RUL) prediction is a pivotal task for making well-informed maintenance decisions. Currently, various approaches have been proposed for RUL prediction, which can be broadly categorized into three types: model-based

Yubo Hou, Yucheng Wang, Min Wu, Xiaoli Li and Zhenghua Chen are with Institute for Infocomm Research (I²R), Agency for Science, Technology and Research (A*STAR), Singapore.

Yubo Hou, Chee-Keong Kwoh and Xiaoli Li are with School of Computer Science and Engineering, Nanyang Technological University, Singapore.

Mohamed Ragab and Abdulla Alseiari are with Propulsion and Space Research Center, Technology Innovation Institute, UAE.

*Corresponding author: Zhenghua Chen

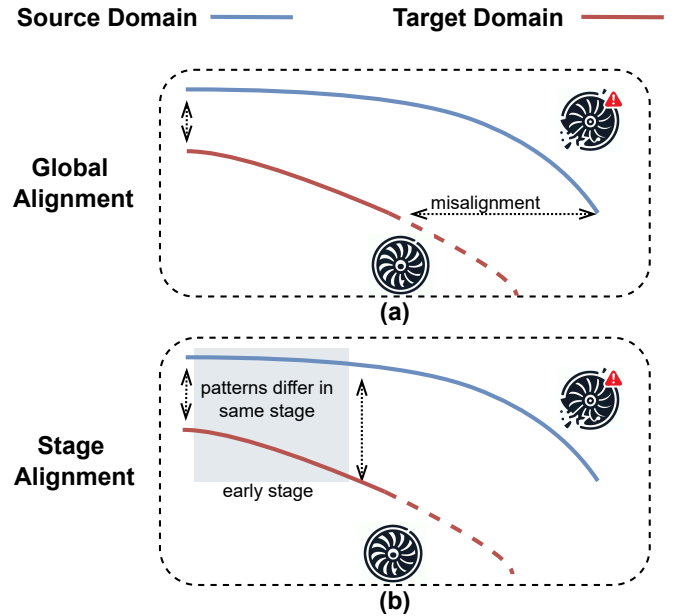


Fig. 1: Comparison of existing solutions and the proposed solution for incomplete degradation domain adaptation in RUL prediction. (a) Under global alignment, early degradation in the target domain may be incorrectly aligned with late stage degradation in the source domain. (b) The patterns of the two domains may differ in the early stage, where the source domain experiences steady degradation, while the target domain degrades rapidly.

approaches, data-driven approaches, and hybrid approaches. Specifically, model-based approaches rely on mathematical or physics-based models to describe the degradation behavior of a system, requiring a strong theoretical understanding [2]. However, as mechanical systems become increasingly complex, predicting RUL using model-based methods becomes exceedingly challenging. With the growing availability of data from deployed sensors, data-driven approaches [3], [4], [5] have gained popularity for RUL prediction.

Despite the promise of data-driven approaches, their success primarily hinges on the assumption of identically distributed data [6]. However, given the dynamics of real-world environments, models are typically trained under one operating condition and tested under another, leading to significant performance degradation due to domain shift. Furthermore, collecting annotated data in new operating conditions and

retraining the model is both impractical and costly. Given these challenges, accurately predicting RULs under various working conditions with limited labeled data poses significant difficulties. To address these obstacles, unsupervised domain adaptation (UDA) has emerged as a promising technique that facilitates knowledge transfer from a labeled source domain to a distinct yet related unlabeled target domain [7]. Recently, there has been an increased focus on UDA for RUL prediction task, aiming to learn domain-invariant features by reducing domain shift either through adversarial training [8], [9], [10] or minimizing the statistical distance between domains [11], [12], [13].

Although current DA methods have proven effective in addressing domain shift in RUL prediction, they are typically designed under the assumption that complete run-to-failure data is available in the target domain. However, in industrial systems, such data is often scarce due to safety concerns, as most systems are not allowed to operate until failure. As a result, the target domain may lack crucial data from the final degradation stage, leaving only data from the early degradation stages available. When existing DA methods are applied in these incomplete settings, they often struggle for two main reasons. First, by not considering the progression of degradation stages, these methods typically achieve global alignment, leading to misalignment across domains. As illustrated in Fig. 1 (a), early degradation in the target domain may align with late degradation in the source domain, causing misalignment. Second, due to varying operating conditions, degradation patterns of different machines may differ even within the same degradation stage [14]. As shown in Fig. 1 (b), the patterns of the two domains differ in the early stage, where the source domain experiences steady degradation, while the target domain degrades rapidly. These differing patterns lead to different feature representations. Strict alignment of such features, even when degradation stages are properly aligned, can negatively impact overall alignment performance.

To address these challenges, we propose a novel evidential adaptation approach, EviAdapt, for RUL prediction with incomplete degradation data in the target domain. To address the misalignment of degradation stage, we introduce a novel approach that segments both source and target domains into distinct degradation stages based on degradation rate, followed by stage-wise alignment of samples. By aligning samples at same degradation stages, our method ensures accurate degradation alignment across domains, addressing a critical limitation in existing DA techniques for RUL prediction. To resolve the issue of strict feature alignment, we propose an evidential uncertainty alignment technique that focuses on aligning uncertainty levels between corresponding degradation stages rather than directly aligning features. Given that uncertainty is a second-order statistical equivalent [15], the consistency in uncertainty levels across corresponding degradation stages can effectively bridge differences between domains, thereby improving the alignment in RUL tasks. Through extensive experiments, we have thoroughly evaluated the performance of our proposed EviAdapt method in accurately predicting the RUL of machines across diverse operating conditions.

The main contributions of this study are listed as follows.

- We propose a stage-wise alignment strategy that aligns sample within the same degradation stage across different domains, effectively addressing the misalignment of degradation stage of incomplete lifecycle data in the target domain.
- We introduce a novel evidential uncertainty alignment technique that aligns uncertainty levels between corresponding degradation stages.
- We conduct extensive experiments on the C-MAPSS, N-CMAPSS and PHM2010 datasets to demonstrate that our EviAdapt approach significantly outperforms existing state-of-the-art methods in cross-domain RUL prediction, validating the effectiveness of our strategies in practical scenarios.

II. RELATED WORKS

A. Unsupervised Domain Adaptation for RUL Prediction

Unsupervised Domain Adaptation (UDA) for RUL prediction aims to mitigate the labeling cost by training neural networks to transfer knowledge from a labeled source domain to an unlabeled target domain. Existing UDA methods strive to achieve high performance on the target domain by minimizing the domain discrepancy. These methods can be categorized into two distinct branches, i.e., metric-based methods and adversarial-based methods.

Metric-based methods enable networks to learn invariant features by enforcing metric constraints. Deep domain confusion (DDC) [16] employs the maximum mean discrepancy (MMD) to address the challenge of domain discrepancy. Correlation alignment (CORAL) [17] focused on minimizing the covariance shift between the feature distributions of the source and target domains.

Adversarial-based methods employ domain discriminator networks to compel the feature extractor to acquire representations that are invariant across domains. Domain adversarial neural network [10] utilized a reverse gradient strategy to conduct adversarial training for both the domain classifier and the feature extractor. Adversarial domain adaptation approach for remaining useful life prediction (ADARUL) [8] utilized a conventional GAN loss with flipped labels to learn domain-invariant features. Contrastive adversarial domain adaptation (CADA) [18] incorporated a contrastive loss to persevere target-specific information for RUL prediction.

The above methods operate under the assumption that the target domain possesses complete run-to-failure data. In reality, acquiring such data in the target domain can be challenging, rendering these methods less effective in practical scenarios. In response to the condition of incomplete target data, Cons DANN [19] utilized a consistency-based regularization term during alignment to mitigate the negative impact of missing information in the incomplete target domain dataset. In [20], the authors proposed a generative adversarial network to generate various types of full-cycle degradation data. However, the aforementioned methods treat training data as a homogeneous whole and overlook the discrepancies in characteristics across different degradation stages between the source and target domains, potentially leading to negative

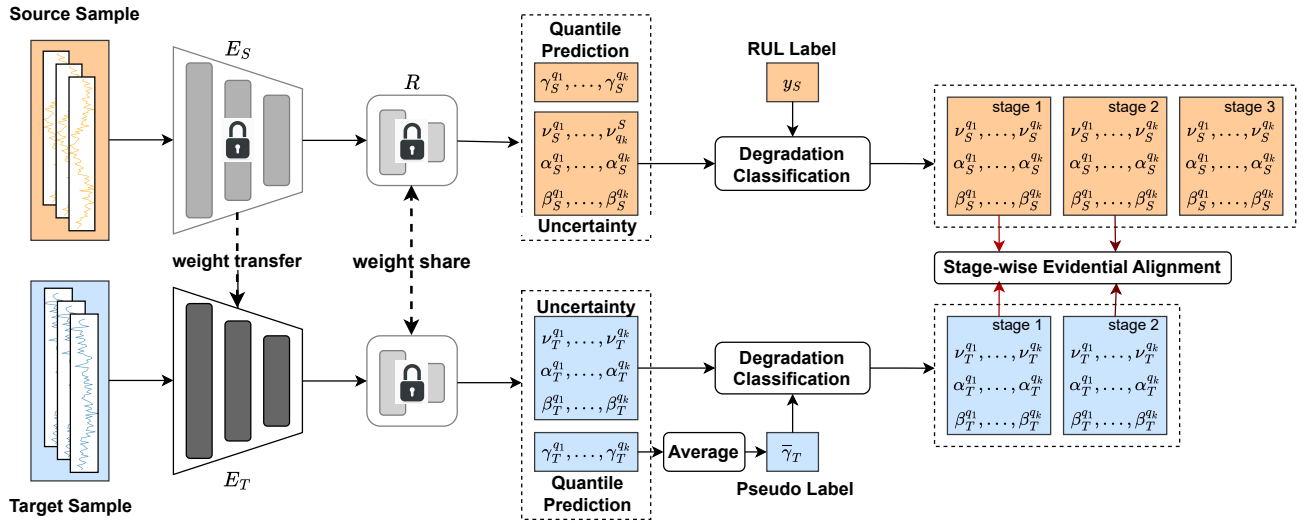


Fig. 2: An overview of our proposed EviAdapt approach. EviAdapt comprises three main components: source encoder E_S , target encoder E_T and shared predictor R . E_S and R are pretrained to learn the RUL distribution and its uncertainty of the source domain using evidential learning. During adaptation, source and target data are segmented into different degradation stages. Eventually, E_T is trained to align the uncertainty of the same degradation stages between the source and target domains.

transfer effects. In [21], the authors proposed an adversarial learning strategy combined with a source-domain instance-weighted degradation fusion scheme for similar degradation levels. However, this method is specifically designed for bearings and lacks generalizability, particularly when applied to aero engine data. Moreover, all these methods ignore the uncertainty when learning the domain distribution.

B. Uncertainty Quantification

Various methods have been developed to estimate uncertainty, including weights reparametrization [22], [23], dropout [24], and ensembling [25]. Although these methods are effective, they are computationally demanding. Evidential learning can estimate uncertainty using single deterministic models. Several works [26], [27], [28] have been proposed for classification tasks. For regression tasks, deep evidential regression [29] was introduced. However, a notable limitation is the reliance on Gaussian assumptions, which may restrict its application. While existing methods primarily rely on evidential learning for uncertainty quantification, our approach leverages uncertainty alignment as a means to reduce the domain gap between source and target.

III. METHODOLOGY

A. Problem Formulation

We denote a source domain with N_S labeled samples $\{X_S^i, y_S^i\}_{i=1}^{N_S}$ and a target domain with N_T unlabeled samples $\{X_T^i\}_{i=1}^{N_T}$, where $X_S^i \in \mathbb{R}^{M \times L}$ and $X_T^i \in \mathbb{R}^{M \times L}$ are both multivariate time series data consisting of M sensors and L time steps. y_S^i is the RUL label. We aim to transfer knowledge from labeled source domain to unlabeled target domain and then improve the performance of RUL prediction on the target. Table I provides a summary of the notations employed in this paper.

TABLE I: List of notations.

Notation	Definition
X_S/X_T	source/target data
y_S	source RUL label
N_S/N_T	number of source/target samples
f_S/f_T	source/target features
E_S/E_T	source/target encoder
R	predictor
M	number of sensors
L	sequence length

B. Overview

The overall structure of our proposed EviAdapt method is illustrated in Figure 2. EviAdapt comprises three main components: source encoder E_S , target encoder E_T and shared predictor R . First, we pretrain source encoder E_S and predictor R to learn the RUL distribution and its uncertainty of the source domain using evidential learning. Second we segment source and target data into different degradation stages. Eventually, we train target encoder E_T to align the uncertainty of the same degradation stages between the source and target domains, leveraging the well-trained E_S and R to facilitate the process.

C. Evidential Pretraining on Source Domain

The first step in our proposed method is to pretrain source encoder and predictor. During this phase, the objective is to train an evidential model using the labeled source domain data to learn the uncertainty of the source domain. Deep evidential regression [29] is a single deterministic forward-pass model that estimates uncertainty under the assumption of Gaussian distribution. This assumption limits the modeling applications. To overcome this limitation, we employ an evidential Bayesian quantile regression model as the RUL predictor [30]. Specifically, a source encoder E_S and a predictor R are trained on

source data X_S . The source encoder extracts features from source data: $f_S = E_S(X_S)$. The predictor estimates the quantile of the RUL value and its uncertainty based on the extracted features.

Assuming that y_S come from a Gaussian distribution parameterized in the form of quantile regression, we place a Gaussian prior on the unknown mean and an Inverse-Gamma prior on the unknown variance [30]:

$$y_S \sim \mathcal{N}(\mu + \tau z, \omega \sigma^2 z), \mu \sim \mathcal{N}(\gamma, \sigma^2 \nu^{-1}), \sigma^2 \sim \Gamma^{-1}(\alpha, \beta) \quad (1)$$

where $\Gamma(\cdot)$ is the Gamma function, $\gamma \in \mathbb{R}, \nu > 0, \alpha > 1, \beta > 0$, $\tau = \frac{1-2q}{q(1-q)}$ and $\omega = \frac{2}{q(1-q)}$ are quantile-specific constants from a specified quantile q , and $z \sim \text{Exp}\left(\frac{1}{\beta/(\alpha-1)}\right)$.

Together, the distributions of μ and σ form the Normal-Inverse-Gamma (NIG) evidential prior [29]:

$$p(\mu, \sigma^2 | \gamma, \nu, \alpha, \beta) = \frac{\beta^\alpha \sqrt{\nu}}{\Gamma(\alpha) \sqrt{2\pi\sigma^2}} \left(\frac{1}{\sigma^2}\right)^{\alpha+1} \exp\left\{-\frac{2\beta + \nu(\gamma - \mu)^2}{2\sigma^2}\right\} \quad (2)$$

The objective is to infer the parameters $(\gamma, \nu, \alpha, \beta)$ of this evidential distribution. By placing the NIG prior on the likelihood parameters, we can derive an analytical solution that produces a Student-t predictive distribution. To learn the parameters of the evidential distribution, we maximize the likelihood of the Student-t distribution. So we minimize the negative log-likelihood loss during training:

$$\mathcal{L}_{NLL} = \frac{1}{2} \log\left(\frac{\pi}{\nu}\right) - \alpha \log(4\beta(1 + \omega \bar{z} \nu)) + \left(\alpha + \frac{1}{2}\right) (\log(y - \gamma - \tau \bar{z})^2 \nu + 4\beta(1 + \omega \bar{z} \nu)) + \log\left(\frac{\Gamma(\alpha)}{\Gamma(\alpha + \frac{1}{2})}\right), \quad (3)$$

where \bar{z} is the mean of z .

A tilted loss is used as regularization term to penalize evidence of prediction errors:

$$\mathcal{L}_R = \max(q(y - \gamma), (q - 1)(y - \gamma)) \Phi, \quad (4)$$

where $\Phi = 2\nu + \alpha + 1/\beta$ is model confidence.

Given a set of quantile value, the source encoder and the RUL predictor are optimized with the negative log-likelihood loss and tilted loss:

$$\mathcal{L} = \sum_{q=1} (\mathcal{L}_{NLL} + \lambda \mathcal{L}_R), \quad (5)$$

We follow the settings described in [29], [30] and enforce the constraints on (ν, α, β) using a softplus activation function, with an additional +1 added to α to ensure $\alpha > 1$. A linear activation function is used for γ .

It is worth noting that the RUL predictor estimates the parameters of the NIG distribution for each quantile value q , given a set of quantile values $[q_1, q_2, \dots, q_k]$:

$$(\gamma_S, \nu_S, \alpha_S, \beta_S) = R(f_S). \quad (6)$$

where $\gamma_S = [\gamma_S^{q_1}, \dots, \gamma_S^{q_k}]$, $\nu_S = [\nu_S^{q_1}, \dots, \nu_S^{q_k}]$, $\alpha_S = [\alpha_S^{q_1}, \dots, \alpha_S^{q_k}]$ and $\beta_S = [\beta_S^{q_1}, \dots, \beta_S^{q_k}]$. And RUL value can be estimated by average of γ_S .

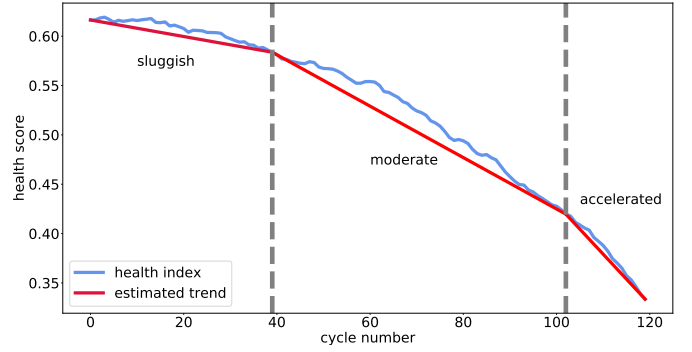


Fig. 3: Three degradation stages categorized by the health index.

D. Stage Segmentation

Given the pretrained source model, the focus lies in achieving adaptation upon the unlabeled incomplete target data. Instead of aligning feature, we align uncertainty between source and target domains. By aligning the uncertainty, we can effectively align conditional distributions, leading to improved domain alignment. However, globally aligning uncertainty overlooks incomplete target domain data situation, leading to suboptimal alignment. To address this issue, we propose a stage segmentation to ensure the alignment of corresponding degradation stages during the adaptation phase. Specifically, we classify the degradation of complete source domain and incomplete target domain into different stages based on their degradation speed.

1) *Identifying Source Degradation Stages*: For the complete source domain, we categorize the data into three stages using the available RUL labels. To accurately define the boundary for each stage, we calculate an engine's "health index" (HI) by forming a linear combination of the key sensor readings, following the methods described in [31], [32]. This curve effectively reflects the overall evolution of the engine's health from normal operation to failure. After obtaining the HI, we examine how it changes over time for each engine, combined with the RUL information, to observe the varying degradation rates in different sections of the lifecycle. Based on the health index, we empirically establish life-cycle ranges of (0, 33%), (33%, 85%), and (85%, 100%) to denote the sluggish, moderate, and accelerated degradation stages, respectively [31], [32]. The reasons for choosing these three ranges are as follows:

- Sluggish stage: The HI curve changes relatively slowly here, indicating that the engine is in a more "healthy" state with a lower degradation rate.
- Moderate stage: As operation time increases, the degradation rate begins to accelerate, though it has not yet entered a high-failure-risk phase. The HI value often shows a marked decline compared to the initial stage.
- Accelerated stage: Near failure, the degradation rate increases significantly, and the HI curve typically exhibits a rapid drop, indicating a steep rise in failure risk.

Figure 3 presents the health index of a single engine across its 120 operational cycles. The full cycle is divided into three distinct stages: the sluggish stage (cycles 0 to 40, corre-

sponding to 0–33%), the moderate stage (cycles 40 to 102, corresponding to 33–85%), and the accelerated stage (cycles 102 to 120, corresponding to 85–100%). The figure clearly shows that the trends in the health index vary significantly across these stages, highlighting the differences in degradation behavior.

2) *Identifying Target Degradation Stages*: For the incomplete target domain, segmenting into the different degradation stages becomes a challenge due to the absence of labels. To address this, we label the target data using the pretrained source model. Due to the incomplete data, it is highly possible that parts of the moderate and fully accelerated degradation stages are missing. Therefore, we classified the data into two stages using pseudo labels. We empirically determine life-cycle ranges of (0, 70%) and (70%, 100%) to represent the sluggish and moderate stages, respectively.

E. Stage-wise Evidential Alignment

After segmentation of the degradation stages, we propose a stage-wise evidential alignment loss \mathcal{L}_{SEA} to align uncertainty levels between corresponding degradation stages rather than directly matching features. The two inputs to this loss are the parameters of the evidential distributions (NIG distributions in our case) from the corresponding degradation stages in the source and target domains.

$$\mathcal{L}_{SEA} = - \sum_{n=1}^2 \mathbb{E}[k((\boldsymbol{\nu}_S, \boldsymbol{\alpha}_S, \boldsymbol{\beta}_S)_n, (\boldsymbol{\nu}_T, \boldsymbol{\alpha}_T, \boldsymbol{\beta}_T)_n)]. \quad (7)$$

$(\boldsymbol{\nu}, \boldsymbol{\alpha}, \boldsymbol{\beta})_n$ represents the parameters of the evidential distribution associated with degradation stage n , where $n = 1$ corresponds to the sluggish stage and $n = 2$ to the moderate stage. The $k(\cdot, \cdot)$ is a kernel function to measure the distance between the evidential parameters from the source and the target domain.

F. Overall Objective

In the EviAdapt algorithm (Algorithm 1), the primary objective is to fine-tune the target encoder E_T for the RUL estimation of equipment. As indicated in Line 1, the algorithm begins with the pretraining of the source encoder E_S and the predictor R using the source domain data (X_S, y_S) . After pretraining, the target domain data X_T are passed through the pretrained source encoder E_S , and the predictor R generates the pseudo labels \hat{y}_T (Line 2 and 3). Next, the source domain data X_S is segmented into three distinct degradation stages, based on the source labels y_S (Line 4). Similarly, the target domain data X_T is segmented into two degradation stages, based on the pseudo labels \hat{y}_T (Line 5). Then the parameters of the evidential distribution $\boldsymbol{\nu}_S, \boldsymbol{\alpha}_S, \boldsymbol{\beta}_S$ for the segmented source domain data are estimated by the predictor R according to the input samples (Line 6 and 7). During the training iteration, the parameters of the evidential distribution $\boldsymbol{\nu}_T, \boldsymbol{\alpha}_T, \boldsymbol{\beta}_T$ for the segmented target domain data are estimated (Line 9 and 10). The source and target parameters of the evidential distribution serve as inputs to the stage-wise evidential alignment loss \mathcal{L}_{SEA} , which is designed to align uncertainty levels between

corresponding degradation stages from the source and target domains, thereby training the target encoder E_T for better adaptation. (Line 11 and 12). Finally, the well trained target encoder E_T can be used in predicting RUL in the target domain.

Algorithm 1: Our Proposed EviAdapt

Input: Source domain: $\{X_S, y_S\}$, Target domain: X_T
Output: Trained target encoder E_T

- 1 $E_S, R \leftarrow \text{pretrain}(X_S, y_S)$
- 2 $\gamma_T, \boldsymbol{\nu}_T, \boldsymbol{\alpha}_T, \boldsymbol{\beta}_T \leftarrow R(E_S(X_T))$
- 3 $\hat{y}_T \leftarrow \text{average } \gamma_T \text{ over } [q_1, q_2, \dots, q_k]$
- 4 $X_{S1}, X_{S2}, X_{S3} \leftarrow \text{stage segmentation for } X_S \text{ based on } y_S$
- 5 $X_{T1}, X_{T2} \leftarrow \text{stage segmentation for } X_T \text{ based on } \hat{y}_T$
- 6 $\gamma_{S1}, \boldsymbol{\nu}_{S1}, \boldsymbol{\alpha}_{S1}, \boldsymbol{\beta}_{S1} \leftarrow R(E_S(X_{S1}))$
- 7 $\gamma_{S2}, \boldsymbol{\nu}_{S2}, \boldsymbol{\alpha}_{S2}, \boldsymbol{\beta}_{S2} \leftarrow R(E_S(X_{S2}))$
- 8 **while iteration do**
- 9 $\gamma_{T1}, \boldsymbol{\nu}_{T1}, \boldsymbol{\alpha}_{T1}, \boldsymbol{\beta}_{T1} \leftarrow R(E_T(X_{T1}))$
- 10 $\gamma_{T2}, \boldsymbol{\nu}_{T2}, \boldsymbol{\alpha}_{T2}, \boldsymbol{\beta}_{T2} \leftarrow R(E_T(X_{T2}))$
- 11 $\text{loss} \leftarrow \mathcal{L}_{SEA}((\boldsymbol{\nu}_S, \boldsymbol{\alpha}_S, \boldsymbol{\beta}_S)_n, (\boldsymbol{\nu}_T, \boldsymbol{\alpha}_T, \boldsymbol{\beta}_T)_n)$
- 12 $\theta_{E_T}^{(t+1)} = \theta_{E_T}^{(t)} - lr \cdot \nabla_{\theta_{E_T}} \text{loss} // \text{Update } E_T \text{ by minimizing loss through backpropagation}$
- 13 **return } E_T**

IV. EXPERIMENTS

A. Data Preparation

We employ the C-MAPSS, N-CMAPSS and PHM2010 benchmark datasets to evaluate the performance of State-of-the-Art methods.

- *C-MAPSS*: This dataset comprises operational data from four different turbofan engines, each functioning under unique operational conditions and exhibiting specific fault modes, as detailed in Table II. It features readings from 21 sensors placed strategically to monitor engine health. To simulate the situation of incomplete target domain data, we excluded the final 40% of the run-to-failure data for each engine in the target training set but kept the full test data, then applied the preprocessing methodology from [18], resulting in a refined dataset that includes data from 14 selected sensors, with labels indicating the engines' remaining useful life.
- *N-CMAPSS*: This dataset [33] documents the run-to-failure trajectories of turbofan engines. Unlike the C-MAPSS dataset, which is confined to standard cruise phase conditions, N-CMAPSS includes simulations of entire flight cycles—climb, cruise, and descent phases—thereby enhancing the fidelity of degradation modeling. These improvements make N-CMAPSS better equipped to capture the complex dynamics present in real systems. For our experiments, we utilize datasets DS01, DS02, and DS03, which provide data from 20 channels, as outlined in Table II. Similarly, we excluded the final 40% of the run-to-failure data for each engine in the target

TABLE II: Details of benchmark datasets.

Dataset	C-MAPSS				N-CMAPSS			PHM2010		
	FD001	FD002	FD003	FD004	DS01	DS02	DS03	C1	C4	C6
# Engine units for training	100	260	100	249	6	6	9	NA		
# Engine units for testing	100	259	100	248	4	3	6	NA		
# Complete Training samples	17731	48558	21220	56815	4881	5237	5532	69176	70270	69054
# Incomplete Training samples	9438	24607	11893	29434	2918	3131	3302	42162	41505	41432
# Testing samples	100	259	100	248	2717	1240	4225	28108	27671	27622

training set while retaining the full test data. The rest preprocessing follows the methodology described in [34].

- *PHM2010*: The PHM2010 dataset [35] provides detailed records of cutting tool wear during machining processes. Due to the strong correlation between the RUL of the cutter and wear, and given that the dataset labels represent the wear depth, the objective is to predict the wear depth of the cutters after each cut [36]. For our experiments, we leverage datasets C1, C4, and C6, as these records include labels for evaluation. Each record, representing the continuous use of the same cutter, contains approximately 315 cutting instances with 7 sensor channels. Additionally, a sliding window has been employed to preprocess the data. As the data is relatively sparse while the dataset is large, a large stride of 1000 has been used to cover the broad range of the whole dataset. Meanwhile, the sliding window of 100 is adopted to reduce computational overhead. The data is normalized to scale all features to the range [0, 1]. For domain adaptation tasks, the first 60% of the cutting instances from the records are used as the target training set, while the remaining 40% are reserved for testing.

B. Experimental Setting

All experiments run five times and the average results are shown to prevent the effect of random initialization. For fair comparisons, we adopt the same LSTM [37] feature extractor for proposed method and baseline methods. Due to the variation between different dataset, different number of layers and different size of hidden states are selected for each dataset. Table III shows the detailed feature extractor parameters for each dataset. Additionally, we set batch size as 256, optimizer as Adam, learning rate as 5e-5 for the target encoder. We use quantile values [0.25, 0.75] in our proposed method to compare with the state-of-the-art methods. Furthermore, we built and trained our model based on Pytorch and NVIDIA GeForce RTX A4000 GPU. We adopt root mean square error (RMSE) and Score [18] as evaluation metrics for the C-MAPSS and N-CMAPSS datasets. Notably, as the Score function has parameters specifically designed for turbofan engine datasets and are not suitable for the PHM2010 dataset, only RMSE has been utilized for measurement. The lower the two indicators are, the better the model is.

The RMSE metric is defined as follows:

$$RMSE = \sqrt{\frac{1}{N} \sum_{i=1}^N (y_i - \hat{y}_i)^2}, \quad (8)$$

where \hat{y}_i and y_i represent the estimated RUL and true RUL respectively.

TABLE III: Parameter setting for the LSTM feature extractor.

Parameter	C-MAPSS	N-CMAPSS	PHM2010
# of Layers	5	1	5
# of Hidden Size	32	64	32
Dropout	0.5	0.1	0.1

The RMSE metric assigns equal importance to both early and late RUL predictions. However, in prognostics applications, late RUL predictions have more detrimental consequences for the systems. In order to address this concern, the Score metric is employed, which imposes a more severe penalty for late RUL predictions. The Score metric is expressed as follows:

$$Score_i = \begin{cases} e^{-\frac{\hat{y}_i - y_i}{13}} - 1; \hat{y}_i < y_i, \\ e^{\frac{\hat{y}_i - y_i}{10}} - 1; \hat{y}_i > y_i, \end{cases} \quad (9)$$

$$Score = \sum_{i=1}^N Score_i. \quad (10)$$

C. Comparison with State-of-the-Art Methods

We compare the proposed EviAdapt with a range of state-of-the-art UDA methods, including conventional domain adaptation methods like DDC [38], Coral [17], ADARUL [8], and CADA [18], as well as Cons DANN [19] which is specifically designed for incomplete domain adaptation in the context of RUL prediction. Further, the results of source only (Source) are also compared. Due to the use of evidential learning for pre-training in the proposed method, the last layer of our predictor differs from other domain adaptation methods. Therefore, we present two sets of source-only results. The first set, Source-RMSE, uses a predictor trained with the RMSE loss. The second set, Source-EVI, employs an evidential predictor trained with negative log-likelihood loss and tilted loss.

Table IV shows the RMSE results and Table V shows the Score results respectively in 12 cross-domain scenarios for RUL prediction on C-MAPSS dataset. From the results, we observe that even though Source-EVI performs significantly worse than Source-RMSE, EviAdapt achieves the best performance in the 8 scenarios for RMSE and in the 9 scenarios for Score. Notably, EviAdapt improves the average performance by over 5% in RMSE and 16% in Score compared to the second-best method.

Similarly, Table VI shows the RMSE and Table VII shows the Score results respectively in 6 cross-domain scenarios for RUL prediction on N-CMAPSS dataset. From the results, we observe that EviAdapt achieves the best performance across

TABLE IV: Comparison of the proposed EviAdapt against benchmark approaches on C-MAPSS (RMSE). Note that F1 is short for FD001, and F1→F2 refers to the scenario where FD001 is the source domain and FD002 is the target domain. Bold indicates the best result, and underline indicates the second-best result.

Methods	F1→F2	F1→F3	F1→F4	F2→F1	F2→F3	F2→F4	F3→F1	F3→F2	F3→F4	F4→F1	F4→F2	F4→F3	Avg.
Source-RMSE	55.35	60.52	55.98	52.29	53.60	54.86	41.94	44.37	40.57	46.09	51.46	49.10	50.51
DDC	40.00	40.06	43.98	38.83	48.24	43.06	41.55	40.65	43.68	40.51	39.61	38.16	41.53
Deep Coral	36.90	41.75	45.21	35.88	41.16	43.85	36.16	37.08	37.78	36.11	36.80	35.96	38.72
ADARUL	44.73	54.37	36.93	48.41	48.84	49.38	34.19	36.19	39.98	28.05	33.76	37.43	41.02
CADA	45.24	54.57	38.73	49.60	49.07	48.74	41.23	39.41	40.55	32.22	39.65	38.17	43.10
Cons DANN	28.52	<u>34.65</u>	29.95	<u>22.86</u>	<u>28.77</u>	<u>29.63</u>	<u>21.02</u>	<u>24.32</u>	27.44	21.21	<u>25.40</u>	<u>23.67</u>	<u>26.45</u>
Source-EVI	59.00	65.83	56.42	56.45	57.77	55.30	54.84	55.48	48.53	46.14	51.34	52.43	54.96
EviAdapt	<u>29.95</u>	31.13	<u>33.72</u>	21.64	26.03	28.83	19.19	19.92	<u>28.53</u>	<u>23.67</u>	18.59	20.58	25.00

TABLE V: Comparison of the proposed EviAdapt against benchmark approaches on C-MAPSS (Score). Note that F1 is short for FD001, and F1→F2 refers to the scenario where FD001 is the source domain and FD002 is the target domain. Bold indicates the best result, and underline indicates the second-best result.

Methods	F1→F2	F1→F3	F1→F4	F2→F1	F2→F3	F2→F4	F3→F1	F3→F2	F3→F4	F4→F1	F4→F2	F4→F3	Avg.
Source-RMSE	75683	46833	72564	16834	23400	67866	6740	25030	19995	11831	46169	13971	35576
DDC	22208	6368	21318	4930	6514	16958	6140	22422	21397	5939	23050	4238	13457
Deep Coral	11782	6723	18697	2986	6802	16098	3001	11538	9907	3033	11495	3416	8790
ADARUL	36618	27370	19401	11467	15171	44955	3862	16706	19380	3207	8913	6032	17757
CADA	37815	27805	24187	13201	15690	47750	6676	22293	19964	4907	13183	6560	20003
Cons DANN	<u>5817</u>	<u>4614</u>	7028	<u>1164</u>	<u>2017</u>	<u>5948</u>	1076	<u>6019</u>	<u>5811</u>	947	<u>4529</u>	<u>1343</u>	<u>3859</u>
Source-EVI	109644	78206	91815	26023	34167	93708	20639	76765	42292	13700	47593	20632	54599
EviAdapt	4976	2435	<u>7456</u>	908	1404	5227	<u>1178</u>	3974	5146	<u>1361</u>	3980	809	3238

TABLE VI: Comparison of the proposed EviAdapt against benchmark approaches on N-CMAPSS (RMSE). Bold indicates the best result, and underline indicates the second-best result.

Methods	DS01→DS02	DS01→DS03	DS02→DS01	DS02→DS03	DS03→DS01	DS03→DS02	Avg.
Source-RMSE	21.89	28.23	33.29	25.64	40.37	26.50	29.32
DDC	19.23	21.12	21.05	15.86	24.75	17.78	19.96
Deep Coral	14.06	15.75	21.34	16.37	24.42	16.21	18.03
ADARUL	9.97	13.50	17.51	14.20	14.07	9.18	13.07
CADA	10.05	14.12	16.07	13.14	18.88	12.90	14.19
Cons DANN	10.03	<u>11.91</u>	<u>16.52</u>	<u>12.96</u>	17.48	10.25	13.19
Source-EVI	23.64	27.89	30.68	24.25	40.23	28.11	29.14
EviAdapt	9.23	9.87	9.69	9.74	9.87	5.81	9.04

TABLE VII: Comparison of the proposed EviAdapt against benchmark approaches on N-CMAPSS (Score). Bold indicates the best result, and underline indicates the second-best result.

Methods	DS01→DS02	DS01→DS03	DS02→DS01	DS02→DS03	DS03→DS01	DS03→DS02	Avg.
Source-RMSE	7202	58571	62615	49246	118257	11480	51228
DDC	5767	28992	16178	14566	24616	5325	15908
Deep Coral	2880	13444	17037	15810	22697	3804	12613
ADARUL	1579	11370	11924	11135	5908	1441	7226
CADA	<u>1632</u>	12260	<u>8568</u>	9814	<u>13335</u>	<u>2459</u>	8011
Cons DANN	1715	<u>8216</u>	9634	<u>9675</u>	10183	1783	<u>6868</u>
Source-EVI	8662	55812	53767	45930	119890	14051	49685
EviAdapt	1515	5742	3804	7553	4205	979	3966

TABLE VIII: Comparison of the proposed EviAdapt against benchmark approaches on PHM2010 (RMSE). Bold indicates the best result, and underline indicates the second-best result.

Methods	C1→C4	C1→C6	C4→C1	C4→C6	C6→C1	C6→C4	Avg.
Source-RMSE	0.209	0.111	0.311	0.201	0.280	0.312	0.237
DDC	0.176	0.272	0.223	0.340	0.127	0.170	0.218
Deep Coral	0.175	0.194	0.155	0.150	0.116	0.169	0.160
ADARUL	<u>0.216</u>	0.114	0.313	0.202	<u>0.300</u>	0.323	0.245
CADA	0.209	0.111	0.311	0.201	0.280	0.312	0.237
Cons DANN	0.173	<u>0.106</u>	<u>0.109</u>	<u>0.118</u>	0.112	0.233	0.142
Source-EVI	0.219	0.112	0.200	0.129	0.259	0.300	0.203
EviAdapt	0.185	0.100	0.105	0.108	0.145	0.192	0.139

TABLE IX: Ablation study for the proposed EviAdapt on C-MAPSS (RMSE).

Alignment Scope	Alignment Type	F1→F2	F1→F3	F1→F4	F2→F1	F2→F3	F2→F4	F3→F1	F3→F2	F3→F4	F4→F1	F4→F2	F4→F3	Avg.
<i>G</i>	<i>Fea</i>	25.47	27.47	34.36	26.11	34.98	36.39	26.87	32.80	33.67	25.42	26.74	25.00	29.61
<i>G</i>	<i>Unc</i>	<u>29.61</u>	32.91	<u>36.00</u>	23.81	31.53	31.50	24.35	24.72	26.45	23.08	24.12	23.83	27.66
<i>S</i>	<i>Unc</i>	29.95	<u>31.13</u>	33.72	21.64	26.03	28.83	19.19	19.92	<u>28.53</u>	<u>23.67</u>	18.59	20.58	25.00

all scenarios with regards to both RMSE and Score. Notably, EviAdapt improves the average performance by over 30% in RMSE and 42% in Score compared to the second-best method.

Moreover, Table VIII shows the RMSE results in 6 cross-domain scenarios for wear depth prediction on PHM2010 dataset. From the results, we observe that EviAdapt achieves the best performance in the 3 scenarios. Notably, EviAdapt improves the average performance by over 2% in RMSE compared to the second-best method.

These consistent superior performances demonstrate EviAdapt’s ability to align uncertainty of the same degradation stage effectively, leading to significant advancements in RUL prediction across different domains.

D. Ablation Study

To validate the contribution of key components, we conducted an ablation study on our proposed EviAdapt using the C-MAPSS dataset. We derived two variants of EviAdapt based on different combinations of alignment scope and alignment type. The alignment scope refers to the range over which the alignment is applied and includes two kinds: global alignment (“*G*”), which considers the entire dataset, and same degradation stage alignment (“*S*”), which focuses on aligning data within the same degradation stage. The alignment type refers to the specific aspect of the data being aligned and includes two kinds: alignment by feature (“*Fea*”) and alignment by uncertainty (“*Unc*”). It is worth noting that the combination (“*S*”, “*Unc*”) corresponds to our proposed method.

Table IX and Table X presents the comparative outcomes between EviAdapt and its variants. Our observations reveal that alignment by uncertainty surpasses alignment by feature, showing an improvement of 65% in terms of average Score. Furthermore, same degradation stage alignment outperforms global alignment, with a maximum improvement of 67% in terms of average Score. These results underscore the effectiveness of stage-wise alignment and alignment by uncertainty.

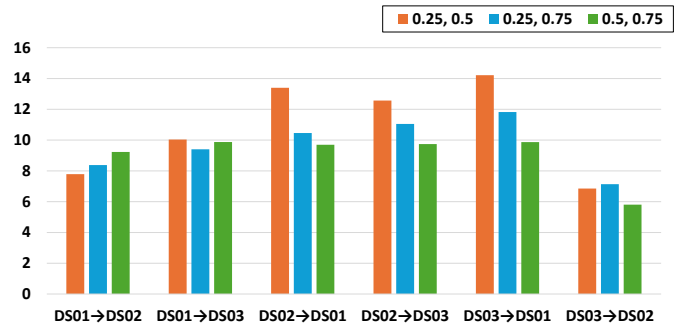


Fig. 4: The sensitivity analysis for different set of quantile values on N-CMAPSS (RMSE).

E. Sensitivity Analysis

We conducted a sensitivity analysis for different set of quantile values q on N-CMAPSS dataset to investigate the impact of evidential learning on the proposed method. Several experiments were carried out using various set of values, including [0.25, 0.5], [0.5, 0.75] and [0.25, 0.75]. Figure 4 and Figure 5 illustrate that the proposed method demonstrates that the optimal set of quantile values varies across different domains. Specifically, the quantiles [0.25, 0.5] yields the best performance for DS01→DS02 in terms of RMSE and Score, while [0.25, 0.5] achieves the best performance for DS02→DS01 and DS02→DS03 in terms of Score. The impact of the quantile values on domain adaptation varies depending on the source and target domains. The potential reason could be attributed to different sets of quantiles capture varying domain information.

F. Visualization of Feature Distribution

To showcase the effectiveness of the proposed method, we employed t-SNE to visualize the latent features in the reduced-dimensional space both before and after adaptation on the N-CMAPSS dataset for the DS01→DS03 scenario. As illustrated in Fig.6, prior to adaptation, a considerable

TABLE X: Ablation study for the proposed EviAdapt on C-MAPSS (Score).

Alignment Scope	Alignment Type	F1→F2	F1→F3	F1→F4	F2→F1	F2→F3	F2→F4	F3→F1	F3→F2	F3→F4	F4→F1	F4→F2	F4→F3	Avg.
<i>G</i>	<i>Fea</i>	3953	2344	35593	7522	11296	59736	27492	94580	80814	3577	8686	2317	28159
<i>G</i>	<i>Unc</i>	6224	2246	8268	3832	7880	29588	6345	26558	15633	891	2608	1093	9264
<i>S</i>	<i>Unc</i>	4976	2435	7456	908	1404	5227	1178	3974	5146	1361	3980	809	3238

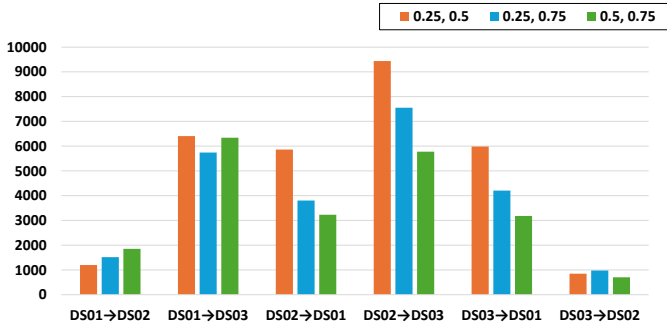


Fig. 5: The sensitivity analysis for different set of quantile values on N-CMAPSS (Score).

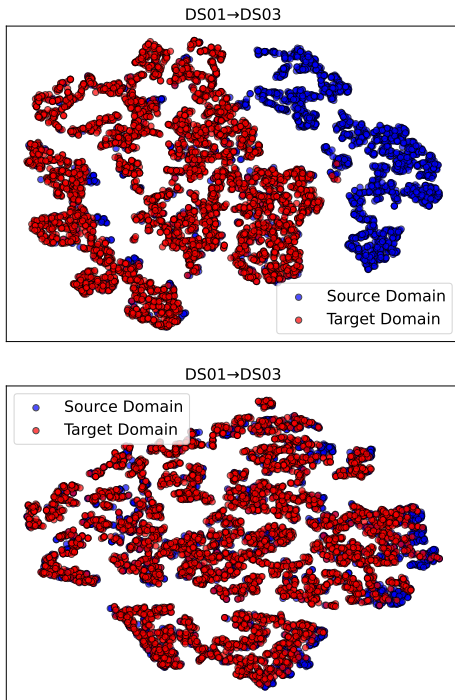


Fig. 6: Feature distribution analysis. Up: before adaptation. Down: after adaptation.

portion of the source samples are positioned far from the target distribution, emphasizing the domain gap. In contrast, post-adaptation visualization demonstrates that the source and target distributions are closely aligned. Collectively, these visualizations clearly indicate that our approach successfully minimizes the disparity between the source and target feature distributions.

V. CONCLUSION

In this paper, we found that most existing domain adaptation methods fail under incomplete target domains. To address this, we propose a novel approach called EviAdapt for unsupervised domain adaptation in RUL prediction tasks. Unlike previous methods that overlook the misalignment of degradation stage and inherent uncertainties in RUL tasks, EviAdapt aligns the uncertainty within the same degradation stage by the proposed stage-wise evidential alignment technique, thereby highlighting the limitations of existing methods. Through extensive experiments, our results demonstrate the remarkable performance of EviAdapt, surpassing state-of-the-art methods on the C-MAPSS, N-CMAPSS, and PHM2010 datasets, with average improvements of 16%, 42%, and 2%, respectively.

In future work, we plan to develop a source-free domain adaptation (SFDA) method for RUL prediction, addressing the challenge of reducing dependencies on fully labeled source domains. In many industrial settings, production data is highly sensitive and often contains confidential information, making it infeasible to share raw data across domains due to corporate privacy policies. Instead, SFDA focuses on adapting pretrained models to target domains without requiring direct access to the source data, ensuring compliance with privacy constraints while maintaining effective domain adaptation.

REFERENCES

- [1] M. Kordestani, M. E. Orchard, K. Khorasan, and M. Saif, "An overview of the state-of-the-art in aircraft prognostic and health management strategies," *IEEE Transactions on Instrumentation and Measurement*, 2023.
- [2] B. Hou, D. Wang, Y. Wang, T. Yan, Z. Peng, and K.-L. Tsui, "Adaptive weighted signal preprocessing technique for machine health monitoring," *IEEE Transactions on Instrumentation and Measurement*, vol. 70, pp. 1–11, 2021.
- [3] H. Zhao, H. Liu, Y. Jin, X. Dang, and W. Deng, "Feature extraction for data-driven remaining useful life prediction of rolling bearings," *IEEE Transactions on Instrumentation and Measurement*, vol. 70, pp. 1–10, 2021.
- [4] C. Chen, N. Lu, B. Jiang, Y. Xing, and Z. H. Zhu, "Prediction interval estimation of aeroengine remaining useful life based on bidirectional long short-term memory network," *IEEE Transactions on Instrumentation and Measurement*, vol. 70, pp. 1–13, 2021.
- [5] L. Ren, H. Qin, Z. Xie, B. Li, and K. Xu, "Aero-engine remaining useful life estimation based on multi-head networks," *IEEE Transactions on Instrumentation and Measurement*, vol. 71, pp. 1–10, 2022.
- [6] W. Mao, J. Liu, J. Chen, and X. Liang, "An interpretable deep transfer learning-based remaining useful life prediction approach for bearings with selective degradation knowledge fusion," *IEEE Transactions on Instrumentation and Measurement*, vol. 71, pp. 1–16, 2022.
- [7] X. Liu, C. Yoo, F. Xing, H. Oh, G. El Fakhri, J.-W. Kang, J. Woo *et al.*, "Deep unsupervised domain adaptation: A review of recent advances and perspectives," *APSIPA Transactions on Signal and Information Processing*, vol. 11, no. 1, 2022.
- [8] M. Ragab, Z. Chen, M. Wu, C. K. Kwok, and X. Li, "Adversarial transfer learning for machine remaining useful life prediction," in *2020 IEEE international conference on prognostics and health management (ICPHM)*. IEEE, 2020, pp. 1–7.

- [9] M. Ragab, E. Eldele, Z. Chen, M. Wu, C.-K. Kwok, and X. Li, "Self-supervised autoregressive domain adaptation for time series data," *IEEE Transactions on Neural Networks and Learning Systems*, vol. 35, no. 1, pp. 1341–1351, 2022.
- [10] P. R. d. O. da Costa, A. Akçay, Y. Zhang, and U. Kaymak, "Remaining useful lifetime prediction via deep domain adaptation," *Reliability Engineering & System Safety*, vol. 195, p. 106682, 2020.
- [11] G. Ma, S. Xu, T. Yang, Z. Du, L. Zhu, H. Ding, and Y. Yuan, "A transfer learning-based method for personalized state of health estimation of lithium-ion batteries," *IEEE Transactions on Neural Networks and Learning Systems*, vol. 35, no. 1, pp. 759–769, 2024.
- [12] H. Cheng, X. Kong, G. Chen, Q. Wang, and R. Wang, "Transferable convolutional neural network based remaining useful life prediction of bearing under multiple failure behaviors," *Measurement*, vol. 168, p. 108286, 2021.
- [13] W. Mao, J. He, and M. J. Zuo, "Predicting remaining useful life of rolling bearings based on deep feature representation and transfer learning," *IEEE Transactions on Instrumentation and Measurement*, vol. 69, no. 4, pp. 1594–1608, 2019.
- [14] X. Li, W. Zhang, H. Ma, Z. Luo, and X. Li, "Degradation alignment in remaining useful life prediction using deep cycle-consistent learning," *IEEE Transactions on Neural Networks and Learning Systems*, 2021.
- [15] J. Wen, N. Zheng, J. Yuan, Z. Gong, and C. Chen, "Bayesian uncertainty matching for unsupervised domain adaptation," in *Proceedings of the 28th International Joint Conference on Artificial Intelligence*, ser. IJCAI'19. AAAI Press, 2019, p. 3849–3855.
- [16] X. Jia, M. Zhao, Y. Di, Q. Yang, and J. Lee, "Assessment of data suitability for machine prognosis using maximum mean discrepancy," *IEEE transactions on industrial electronics*, vol. 65, no. 7, pp. 5872–5881, 2017.
- [17] B. Sun, J. Feng, and K. Saenko, "Correlation alignment for unsupervised domain adaptation," *Domain adaptation in computer vision applications*, pp. 153–171, 2017.
- [18] M. Ragab, Z. Chen, M. Wu, C. S. Foo, C. K. Kwok, R. Yan, and X. Li, "Contrastive adversarial domain adaptation for machine remaining useful life prediction," *IEEE Transactions on Industrial Informatics*, vol. 17, no. 8, pp. 5239–5249, 2020.
- [19] S. Siahpour, X. Li, and J. Lee, "A novel transfer learning approach in remaining useful life prediction for incomplete dataset," *IEEE Transactions on Instrumentation and Measurement*, vol. 71, pp. 1–11, 2022.
- [20] H. Cheng, X. Kong, Q. Wang, H. Ma, S. Yang, and K. Xu, "Remaining useful life prediction combined dynamic model with transfer learning under insufficient degradation data," *Reliability Engineering & System Safety*, vol. 236, p. 109292, 2023.
- [21] X. Li, W. Zhang, X. Li, and H. Hao, "Partial domain adaptation in remaining useful life prediction with incomplete target data," *IEEE/ASME Transactions on Mechatronics*, 2023.
- [22] C. Blundell, J. Cornebise, K. Kavukcuoglu, and D. Wierstra, "Weight uncertainty in neural network," in *International conference on machine learning*. PMLR, 2015, pp. 1613–1622.
- [23] D. P. Kingma, T. Salimans, and M. Welling, "Variational dropout and the local reparameterization trick," *Advances in neural information processing systems*, vol. 28, 2015.
- [24] Y. Gal and Z. Ghahramani, "Dropout as a bayesian approximation: Representing model uncertainty in deep learning," in *international conference on machine learning*. PMLR, 2016, pp. 1050–1059.
- [25] B. Lakshminarayanan, A. Pritzel, and C. Blundell, "Simple and scalable predictive uncertainty estimation using deep ensembles," *Advances in neural information processing systems*, vol. 30, 2017.
- [26] M. Sensoy, L. Kaplan, and M. Kandemir, "Evidential deep learning to quantify classification uncertainty," *Advances in neural information processing systems*, vol. 31, 2018.
- [27] A. Malinin and M. Gales, "Predictive uncertainty estimation via prior networks," *Advances in neural information processing systems*, vol. 31, 2018.
- [28] —, "Reverse kl-divergence training of prior networks: Improved uncertainty and adversarial robustness," *Advances in Neural Information Processing Systems*, vol. 32, 2019.
- [29] A. Amini, W. Schwarting, A. Soleimany, and D. Rus, "Deep evidential regression," *Advances in neural information processing systems*, vol. 33, pp. 14927–14937, 2020.
- [30] F. B. Hüttel, F. Rodrigues, and F. C. Pereira, "Deep evidential learning for bayesian quantile regression," *arXiv preprint arXiv:2308.10650*, 2023.
- [31] Y. Lei, N. Li, L. Guo, N. Li, T. Yan, and J. Lin, "Machinery health prognostics: A systematic review from data acquisition to rul prediction," *Mechanical systems and signal processing*, vol. 104, pp. 799–834, 2018.
- [32] J. Liu, F. Lei, C. Pan, D. Hu, and H. Zuo, "Prediction of remaining useful life of multi-stage aero-engine based on clustering and lstm fusion," *Reliability Engineering & System Safety*, vol. 214, p. 107807, 2021.
- [33] M. Arias Chao, C. Kulkarni, K. Goebel, and O. Fink, "Aircraft engine run-to-failure dataset under real flight conditions for prognostics and diagnostics," *Data*, vol. 6, no. 1, 2021.
- [34] H. Mo and G. Iacca, "Multi-objective optimization of extreme learning machine for remaining useful life prediction," in *Applications of Evolutionary Computation: 25th European Conference, EvoApplications 2022, Held as Part of EvoStar 2022, Madrid, Spain, April 20–22, 2022, Proceedings*. Springer, 2022, pp. 191–206.
- [35] "Phm society 2010 phm society conference data challenge," 2010. [Online]. Available: https://phmsociety.org/phm_competition/2010-phm-society-conference-data-challenge/
- [36] X. Qin, W. Huang, X. Wang, Z. Tang, and Z. Liu, "Real-time remaining useful life prediction of cutting tools using sparse augmented lagrangian analysis and gaussian process regression," *Sensors*, vol. 23, no. 1, p. 413, 2022.
- [37] S. Hochreiter and J. Schmidhuber, "Long short-term memory," *Neural computation*, vol. 9, no. 8, pp. 1735–1780, 1997.
- [38] E. Tzeng, J. Hoffman, N. Zhang, K. Saenko, and T. Darrell, "Deep domain confusion: Maximizing for domain invariance," *arXiv preprint arXiv:1412.3474*, 2014.